Multicolor and Warm White Emissions with a High Color Rendering Index in a Tb^{3+}/Eu^{3+}-Codoped Phosphor Ceramic Plate

Haggeo Desirena [1,*] , **Jorge Molina-González** [1], **Octavio Meza** [2], **Priscilla Castillo** [1] **and Juan Bujdud-Pérez** [1]

1   Centro de Investigaciones en Óptica A.C., A.P. 1-948, León 37150, Mexico
2   Instituto de Física, "Ing. Luis Rivera Terrazas", Benemérita Universidad Autónoma de Puebla, Apartado Postal J-48, Puebla 72570, Mexico
*   Correspondence: hagdes@cio.mx; Tel.: +52-477-414200

check for updates

Abstract: A series of Tb^{3+}/Eu^{3+}-codoped phosphor ceramic plates with a high color rendering index (CRI) for a near-ultraviolet light emitting diode (LED) were fabricated. Color emission can be tuned from green to reddish as a function of Eu^{3+} concentration. By doping only 0.15 mol% of Eu^{3+} concentration, a comfortable warm white emission is promoted as a result of simultaneous emissions of Tb^{3+} and Eu^{3+} ions. A theoretical model is proposed to calculate the contributions of the emitted color of the donor (Tb^{3+}) and acceptor (Eu^{3+}) ions in terms of europium concentration. The energy transfer from Tb^{3+} to Eu^{3+} ions is corroborated by the luminescence spectra and decay time of Tb^{3+}, with a maximum energy transfer efficiency of 76% for 28 mol% of Tb^{3+} and 14 mol% of Eu^{3+}. Warm white LEDs were constructed using a 380 nm UV chip and showed a CRI of 82.5, which was one of highest values reported for Tb^{3+}/Eu^{3+}-codoped samples. Color-correlated temperature (CCT), color coordinate (CC), and luminous efficacy (LE) were utilized to know the potentials as a phosphor converter in solid-state lighting.

Keywords: Luminescence; Tb^{3+}/Eu^{3+}; white light; Luminous efficacy; high CRI; solid state lighting

1. Introduction

In the last decade, phosphor-converted light emitting diodes (pcLEDs) have been introduced into the market to conquer the deficiencies of fluorescent and incandescent lamps. Current pcLEDs are basically a mixture of a phosphor converter and a silicon binder placed in the top of a blue LED chip (InGaN), and the combination of both colors yields white light. However, silicon binders that support the phosphor still present innate issues, such yellowing problems when exposed to a high density of energy caused by their low thermal conductivities [1]. In that sense, luminescence glasses, glass ceramics, phosphor in glass, and ceramic phosphor plates have emerged as good candidates to replace the silicon binder in high-power LEDs [2–5]. Among these approaches, special attention has concentrated on ceramic phosphor plates because of their superior thermal stability over different approaches for solid-state lighting [6]. It exhibits robustness, a homogenous luminescence emission, chemical stability, ageing resistance, and good thermal conductivity. The last property is key for the development of stable high-power LEDs and can be controlled through network formers, network modifiers, and network intermediators [7,8]. Even though this system shows attractive thermal and optical properties, most of the high-power systems using one single phosphor do not meet the characteristics for satisfactory color rendering index (CRI) and low color-correlated temperature (CCT) for residential lighting applications [9,10]. In that sense, a second phosphor to compensate the weak red emission of YAG:Ce^{3+}

has been introduced, and the combination of both phosphors leads to warm white devices with low CCT and improved CRI [11].

Terbium (Tb^{3+}) and europium (Eu^{3+}) ions show prominent emission peaks in green and red regions, respectively. Such ions have been often used as phosphors in cathode ray tubes, plasma display panels, X-ray scintillation screens, and fluorescent lamps [12]. Recently, Eu^{3+}-activated phosphors have been proposed as a new red emitter to compensate for the weak red emission of YAG:Ce^{3+}-based pcLEDs. Results show that by choosing a proper host matrix, Eu^{3+} presents superior photometric properties compared to commercial CASN:Eu^{2+} phosphors under blue and UV excitation [13,14]. The narrow reabsorption of Eu^{3+} is the main advantage over nitride phosphors.

Tb^{3+}/Eu^{3+}-codoped materials such as glass, glass ceramic, and phosphor powder have been demonstrated to produce warm and cold white emission through energy transfer from Tb^{3+} to Eu^{3+} ions. Indeed, color emission and full conversion from green to red can be achieved by changing the ratio of the Tb^{3+} and Eu^{3+} concentration [15–21]. However, energy transfer efficiency and radiative decay probability depend strongly on the phonon energy of the host. Therefore, different promising host materials, such as oxides, oxysulfides, oxynitrides, chloride, and fluoride, have been investigated to develop efficient phosphors [22–26]. In that sense, special attention should be given to inorganic fluorides because of their low phonon energies that promote a decrease in the nonradiative decay probability. Presently, an $NaYF_4$ fluoride crystal is one of the most efficient materials to produce upconversion emission as well as good chemical stability. However, tetragonal-phase $LiYF_4$ crystals exceed the optical properties of $NaYF_4$ because they promote stronger upconversion emissions and generate UV emission lines [27]. The crystalline phases of several $LiYF_4$ samples have been synthetized by thermal decomposition, sol-gel, and Bridgman methods [28–30]. However, with these approaches it is impossible to sinter a phosphor plate. In that sense, a melt-quenching method shows greater potential than the methods mentioned above to synthetize phosphor plates with the desired shape and crystalline phase. These properties make $LiYF_4$ an excellent host for Tb^{3+}/Eu^{3+} ions to be used in solid-state lighting applications.

In spite of several works that show that Tb^{3+}/Eu^{3+}-codoped materials are good candidates for solid-state lighting applications, most of the published reports only present spectroscopic and structural properties. However, luminous efficacy, lighting properties, and device prototypes based in Tb^{3+}/Eu^{3+}-codoped material for solid-state lighting have been seldom reported [31]. In this work, the color tuning of a Tb^{3+}/Eu^{3+} ceramic phosphor plate as a function of Eu^{3+} concentration has been investigated. Color coordinate and color rendering indexes were measured to evaluate the potential of the phosphor converter in solid-state lighting.

2. Materials and Methods

Several $LiY_{1-x-y}F_4$:yTb^{3+}/xEu^{3+} ceramic phosphor plates were prepared by a melt-quenching technique (where y = 28 mol% and x = 0.15, 0.3, 1.5, 8.5, and 14 mol%). In the composition, 5 mol% extra of TeO_2 was used as a sintering additive to promote the formation of a ceramic plate. The total lanthanide concentration in the host matrix and other optical properties are show in Table 1. All reactants were 99.99% pure and used as received. The reactants were tellurium oxide (TeO_2), lithium fluoride (LiF), yttrium fluoride (YF_3), terbium fluoride (TbF_3), and europium fluoride (EuF_3). Calculated quantities of the chemicals were mixed in an agate mortar for 30 min and melted in a PDI electric furnace at 1100 °C for 1 h in alumina crucibles so that a homogeneously mixed melt was obtained. The reaction performance was 96%, indicating a low volatility of fluoride compounds. The samples were subsequently annealed at a temperature of 280 °C. The time to finish the annealing process took around 18 h. Samples were cut and then polished to 800 μm-thick slabs for different measurements. Photoluminescence characterizations were performed using a xenon lamp, monochromator 2300i from Acton Research (Trenton, NJ, USA) and R955 Hamamatsu photomultiplier tube (Hamamatsu, Japan). The decay profile (lifetime) corresponding to 545 nm and 613 nm was recorded using a pulsed UV LED (Opulent Americas, Raleigh, NC, USA) centered at 365 nm and a Teledyne LeCroy oscilloscope (HDO

5055, New York, NY, USA). Special care was taken to maintain the alignment of the set-up in order to compare the intensity of the visible signal between different characterized samples. The ceramic phosphor plate was placed on a commercial UV LED with an emission wavelength centered in 380 nm. An integrating sphere 1 m in diameter (Labsphere Co., North Sutton, NH, USA) was used to measure the CCT, CIE (Comission Internationale de l´Éclairage 1931) chromaticity diagram, color coordinates, and luminous efficacy (LE) with a bias current of 20 mA.

Table 1. Decay time, energy transfer, color coordinate (CC), color-correlated temperature (CCT), color rendering index (CRI), and luminous efficacy (LE) of the ceramic phosphor plate as a function of Eu^{3+} content.

Tb^{3+}/Eu^{3+} (mol%)	$\tau_{Tb}(^5D_4)$ (ms)	ET (%)	x	y	CCT (K)	CRI	LE (lm/W)
28	4.3	0	0.369	0.602	5497	34.06	13.08
28/0.15	4.28	0.4	0.459	0.521	3658	74.81	9.22
28/0.3	4.28	0.4	0.482	0.500	3136	82.54	8.13
28/1.5	3.44	20	0.534	0.453	2225	82.59	7.09
28/8.5	1.42	66	0.614	0.381	1136	42.81	7.80
28/14	0.93	78	0.629	0.368	1294	35.54	6.04

The crystalline structures of the samples were characterized using the X-ray diffraction (XRD) of Bruker instrument (D2 Phaser, Bruker, Billerica, MA, USA) equipment with Cu Kα radiation at 1.54184 Å. The recorded XRD diffractograms were obtained from 10 to 70° 2θ range with increments of 0.02° and a sweep time of 0.5 s. The SEM images were performed using a SEM of JEOL (JSM-7800F, Tokyo, Japan).

3. Results and Discussion

3.1. X-ray Diffraction (XRD) Characterization and Photoluminescence Properties

The composition and phase purity of Tb^{3+}-doped and Tb^{3+}/Eu^{3+}-codoped samples with different rare earth concentrations were analyzed by XRD. As presented in Figure 1a, almost all diffraction peaks from the ceramic phosphor plate could be indexed to the standard tetragonal $LiYF_4$ phase (PDF#77-0816) with low impurity phases, indicating that the samples were successfully crystallized, and TeO_2 concentrations did not cause significant changes in the host structure. According to Figure 1a, it was confirmed that $LiYF_4$ samples possessed a tetragonal crystal structure with space group I41/a. The obtained results were comparable to those reported by Kim et. al., where the tetragonal phase appeared as the main crystalline phase when the Eu^{3+} concentration was below 40 mol% in the $LiYF_4$ matrix [28]. For this study, the total lanthanide concentrations in $LiYF_4$ samples were 28, 28.15, 28.3, 29.5, 36.5, and 42 mol%. Additional impurity peaks appeared from 28 to 29.5 mol%, which were associated with a $Y_2Te_6O_{15}$ (PDF#37-1393) phase, whereas from 36.5 to 42 mol% the peak centered at $2\theta = 28.2°$ disappeared, and the purity of the tetragonal phase increased. The lanthanide concentration also modified the diffraction peaks, shifting to a high angle side, when the lanthanide increased from 28 mol% to 42 mol%. Such a fact was associated with the substitution of larger ionic radii of Tb^{3+} and Eu^{3+} by a smaller Y^{3+} ionic radius. An SEM image of 28 mol% of Tb^{3+}, 28 mol% of Tb/0.15 mol% of Eu, and 14 mol% of Eu^{3+} are shown in Figure 1b. The increase in Eu^{3+} concentration did not promote a significant change on the surface of the phosphor plate.
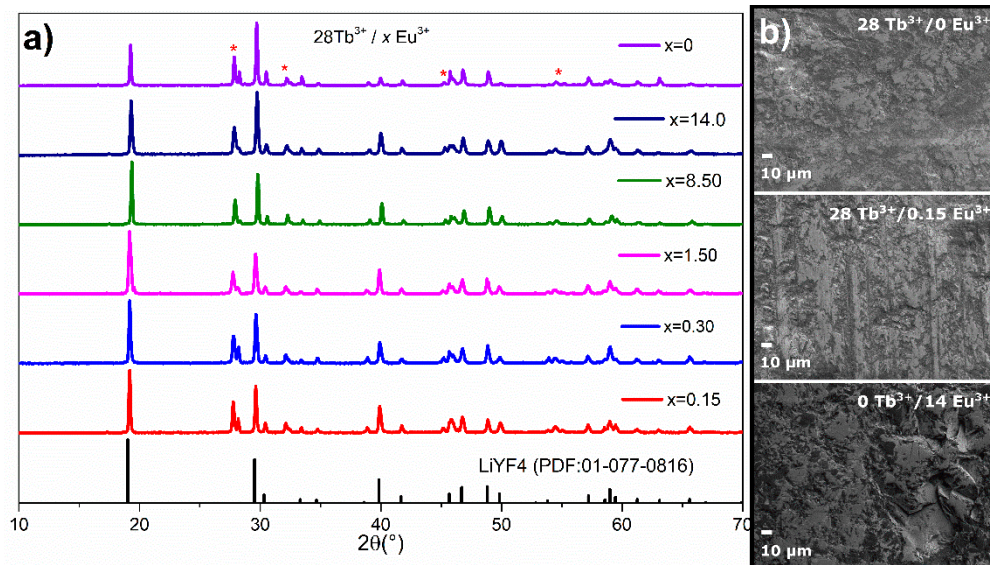
Figure 1. (**a**) X-ray diffraction pattern of the phosphor ceramic plate. The peaks marked with an asterisk correspond to the phase $Y_2Te_6O_{15}$. (**b**) SEM image of the ceramic phosphor plate synthetized trough melt quenching method.

Figure 2a shows the photoluminescence excitation (PLE) from 325 to 500 nm in Tb^{3+}- and Eu^{3+}-doped ceramic plates monitored at 544 and 614 nm, respectively. The spectrum shows four main excitation bands centered at 353, 373, 378, and 485 nm, which were assigned to $^7F_6{\rightarrow}^5D_2$, $^7F_6{\rightarrow}^5L_{10}$, $^7F_6{\rightarrow}^5D_3$, and $^7F_6{\rightarrow}^5D_4$ transitions of Tb^{3+} respectively [29]. The $^7F_6{\rightarrow}^5D_3$ transition showed two excitation peaks at 373 and 378 nm, with the 378 nm shoulder being slightly weaker. From 331 to 338 nm there was a continuous excitation, while from 388 to 475 nm no excitation peaks were observed in Tb^{3+}-doped samples. Figure 2b shows the photoluminescence emission (PL) of Tb^{3+}-doped and Eu^{3+}-doped ceramic phosphor plates under 373 and 396 nm excitation wavelengths. The bands centered at 490, 545, 589, and 622 nm were assigned to $^5D_4{\rightarrow}^7F_6$, $^5D_4{\rightarrow}^7F_5$, $^5D_4{\rightarrow}^7F_4$, and $^5D_4{\rightarrow}^7F_3$ transitions of Tb^{3+} respectively. These visible bands were the result of the well-known down-conversion process, and their emitted colors depended on the concentration of Tb^{3+} ions. In this work, the Tb^{3+} concentration was varied systematically (not show here) from 2 to 28 mol%, and results showed that there was no quenching concentration indicium. These results were similar to those found by other research groups, where 40 mol% of dopant ions were incorporated, and the green emission (545 nm) was the dominant color for the $LiYF_4$ matrix. The inset in Figure 2a shows the picture of the opaque ceramic phosphor plate.
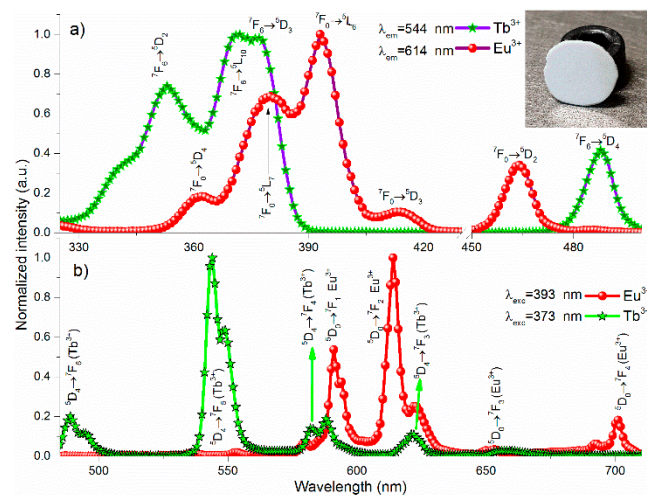
Figure 2. (**a**) Excitation and (**b**) emission spectra for Eu^{3+}- and Tb^{3+}-doped samples. The inset shows the picture of the opaque ceramic phosphor plate.

To distinguish the PLE spectra of Tb^{3+} and Eu^{3+}, a 14 mol% of Eu^{3+}-doped sample was synthesized. Figure 2a shows the excitation spectra of the Eu^{3+}-doped ceramic phosphor plate recorded at 614 nm emission. The sample showed five dominant bands centered at 362, 380, 393, 414, and 464 nm, which were assigned to $^7F_0{\rightarrow}^5D_4$, $^7F_0{\rightarrow}^5L_7$, $^7F_0{\rightarrow}^5L_6$, $^7F_0{\rightarrow}^5D_3$, and $^7F_0{\rightarrow}^5D_2$ transitions of Eu^{3+} respectively. Upon excitation at 393 nm, a magenta color appeared, with a spectral range from 585 to 710 nm, which are shown in Figure 2b. The 592, 614, 653, and 701 nm bands were attributed to $^5D_0{\rightarrow}^7F_1$, $^5D_0{\rightarrow}^7F_2$, $^5D_0{\rightarrow}^7F_3$, and $^5D_0{\rightarrow}^7F_4$ transitions of Eu^{3+}, respectively, where the 592 and 614 nm emission bands were the feature emissions for $LiYF_4$:Eu^{3+}. Among these transitions, the electric dipole $^5D_0{\rightarrow}^7F_2$ transition was the most intense, followed by less intense magnetic dipole $^5D_0{\rightarrow}^7F_1$ transitions. This indicated that Eu^{3+} ions were located at noninversion symmetric sites [32]. An attractive detail of the emission spectrum was observed at the 701 nm band, which typically was 40% less intense than the 614 nm band in the $LiYF_4$ matrix [28]. However, in this work the 701 nm band was debilitated, as it was 78% weaker than 614 nm band. For solid-state lighting applications, the 701 nm band is a waste of energy because the eye sensitivity is zero, whereas 614 nm bands are considered the optimal red emission to obtain high luminous efficacy and high CRI in warm white LEDs [33].

Figure 3 shows the excitation spectra of the Tb^{3+}/Eu^{3+}-codoped ceramic phosphor plate. By adding only 0.15 mol% of Eu^{3+} to the Tb^{3+}-doped sample, the intensity ratios between splitting peaks at 373 and 378 nm changed slightly, where the shoulder at 378 nm was more intense. This fact was due to the spectral overlapping of the excitation bands at 373 and 380 nm of Tb^{3+} and Eu^{3+} ions, respectively. Such bands became more pronounced when the Eu^{3+} concentration increased from 0.05 to 5 mol%. From the point of view of solid-state lighting, the red shift of the excitation bands became significant because the optical power in the commercial LED chip at 380 nm was higher than 365 nm, and there was a lower probability of dispersion at larger wavelengths. In addition, upon 378 nm excitation, both Tb^{3+} and Eu^{3+} were excited efficiently (vertical gray line), producing simultaneously green and red emission bands. As a result, a higher luminous flux was obtained from a phosphor converter device. As presented in Figure 2b, the excitation bands at 378, 393, 464, and 485 nm for Tb^{3+}/Eu^{3+}-codoped samples increased with the Eu^{3+} concentration; however, the intensity of the band at 393 nm depended strongly on Eu^{3+} content rather than the other bands.
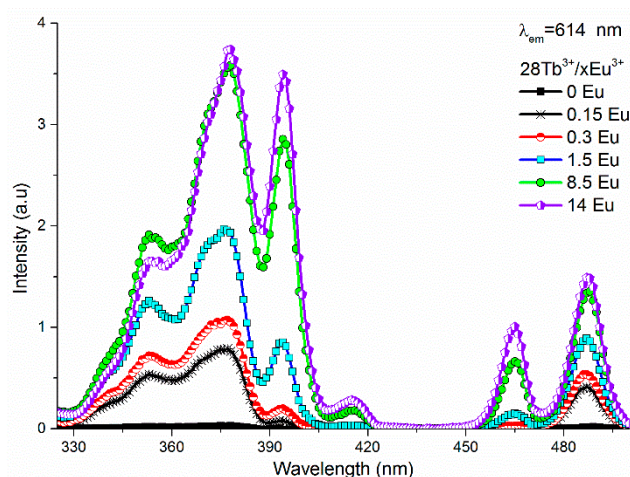
Figure 3. Excitation spectra of the Tb^{3+}/Eu^{3+}-codoped ceramic phosphor plate monitored at 614 nm.

Figure 4 shows the emission spectra of Tb^{3+}/Eu^{3+}-codoped samples as a function of Eu^{3+} concentration. Simultaneous emissions from Tb^{3+} and Eu^{3+} were observed under 378 nm, which indicated the existence of energy transfer between Tb^{3+} and Eu^{3+}. Intensity of emission bands of Tb^{3+} at 490, 545, and 589 nm decreased monotonically as the Eu^{3+} concentration increased from 0.15 mol% to 14 mol%. Among these bands, the 545 nm emission was the most influenced band by Eu^{3+} content, which decreased 36% of the initial intensity with only 0.15 mol% of Eu^{3+}. Concurrently, an increment of 33% was observed for the 614 nm emission band of Eu^{3+} ions. Figure 4 shows that almost all energy was transferred from Tb^{3+} to Eu^{3+} when the Eu^{3+} reached 14 mol%, where red was the main color.
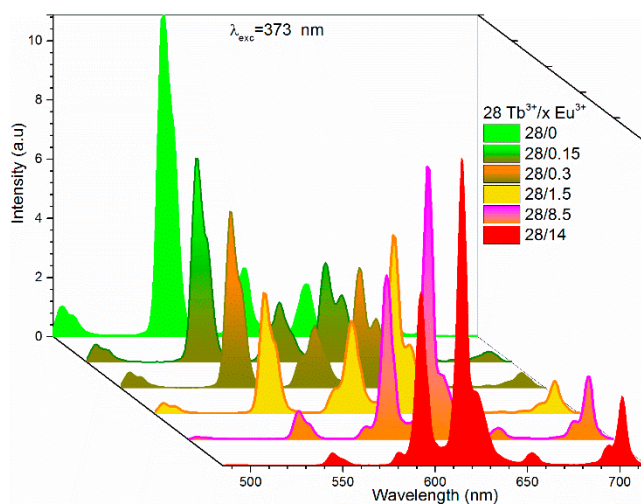

Figure 4. Emission spectra of the Tb^{3+}/Eu^{3+}-codoped ceramic phosphor plate excited at 378 nm.

3.2. Rate Equation Model and Energy Transfer

To clarify the emissions corresponding to Tb^{3+} and Eu^{3+} ions, the following simplified model was proposed. (1) First, some Tb^{3+} ions were promoted from the ground state $^7F_6$ to the excited $^5D_3$ level as a result of pumping at 373 nm. The absorption rate was denoted by A_{02} (s^{-1}). (2) Once some Terbium ions were in the $^5D_3$ level, they relaxed nonradiatively to the $^5D_4$ level; this multiphonon relaxation was denoted by A_{21} (s^{-1}). Subsequently, two processes could occur, phonon relaxation A_{10} (s^{-1}) or energy transfer from Tb^{3+} to Eu^{3+} ions (W). (3) Tb^{3+} emission wavelength peaks were 490, 545, 589, and 622 nm. (4) The energy transfer promotes some Eu^{3+} ions from the $^7F_0$ ground state to $^5D_0$

level where the emission rates B_{10} (s^{-1}) of Eu^{3+} occurred in the 592, 614, 653, and 701 nm peaks, as is shown in Figure 5.
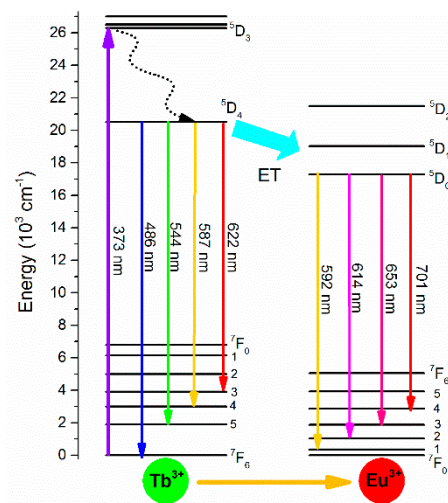

Figure 5. Schematic level diagram of Tb^{3+} and Eu^{3+} and the energy transfer mechanism.

Therefore, the following ratio equations are proposed:

$$\frac{dN_{Tb}^2}{dt} = A_{02}N_{Tb}^0 - A_{21} \tag{1}$$

$$\frac{dN_{Tb}^1}{dt} = A_{21}N_{Tb}^2 - A_{10}N_{Tb}^1 - WN_{Eu}^0 N_{Tb}^1 \tag{2}$$

$$\frac{dN_{Eu}^1}{dt} = -B_{10}N_{Eu}^1 + WN_{Eu}^0 N_{Tb}^1 \tag{3}$$

where N_{Tb}^2, N_{Tb}^1, and N_{Tb}^0 (ions/cm^3) are the Tb^{3+} ion populations in the $^5D_3$, $^5D_4$, and $^7F_6$ energy levels, respectively. N_{Eu}^1 and N_{Eu}^0 (ions/cm^3) are the Eu^{3+} ion populations in the $^5D_0$ and $^1F_0$ levels, respectively. For low-excitation pumping, the ground populations are proportional to the nominal concentration, i.e., $N_{Tb}^0 \approx N_{Tb}$ and $N_{Eu}^0 \approx N_{Eu}$. In stationary conditions the solutions are:

$$N_{Tb}^1 = \frac{A_{02}N_{Tb}}{(WN_{Eu} + A_{01})} \tag{4}$$

$$N_{Eu}^1 = \frac{WA_{02}N_{Tb}N_{Eu}}{B_{10}(WN_{Eu} + A_{01})} \tag{5}$$

$$N_{Tb}^2 = \frac{N_{Tb}A_{02}}{A_{21}} \tag{6}$$

Then, ion populations are related to the emission spectrum by:

$$N_{Tb}^1 = k \int I_{Tb} d\lambda \tag{7}$$

$$N_{Eu}^1 = k \int I_{Eu} d\lambda \tag{8}$$

where I_{Tb} and I_{Eu} are the emission spectra related to the Tb^{3+} and Eu^{3+} emission transitions, and k is a proportional constant. Thus, to obtain the I_{Tb} and I_{Eu} emission spectra, deconvolution of the spectra was performed for both ions, as is shown in Figure 6. Then, we define:

$$P_{Tb} = \frac{N_{Tb}^1}{N_{Tb}^1 + N_{Eu}^1} = \frac{B_{10}}{WN_{Eu} + B_{10}} \tag{9}$$

$$P_{Eu} = \frac{B_{21}N_{Eu}^1}{N_{Tb}^1 + N_{Eu}^1} = \frac{WN_{Eu}}{WN_{Eu} + B_{10}} \tag{10}$$

$$P_{Tb} = \frac{\int I_{Tb}d\lambda}{\int I_{Tb}d\lambda + \int I_{Eu}d\lambda} \tag{11}$$

$$P_{Eu} = \frac{\int I_{Eu}d\lambda}{\int I_{Tb}d\lambda + \int I_{Eu}d\lambda} \tag{12}$$
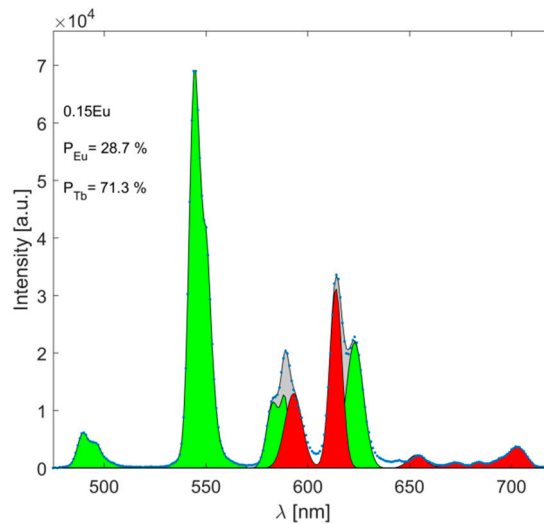

Figure 6. Deconvolution to the experimental emission spectrum (blue). Red and green areas represent the emissions related to the Eu^{3+} and Tb^{3+} ions, respectively.

On the other hand, the dynamic solution for Tb^{3+} in the level $^5D_4$ is:

$$N_{Tb}^1(t) = \frac{A_{21}A_{02}N_{Tb}^0}{A_{21} - A_{10} - N_{Eu}^0 W}\left(e^{-(A_{01}+WN_{Eu}^0)t} - e^{-A_{21}t}\right) \tag{13}$$

This equation has two terms related to the rise time and lifetime. In this way, the lifetime is expressed by:

$$\tau = \frac{1}{A_{01} + WN_{Eu}^0} \tag{14}$$

Figure 7 shows the experimental lifetime curves, and the inset graph is the experimental fitting of Equation (14), with A_{01} = 226.8/s and W = 53.4/s mol%. In our samples, the lifetimes of the $^5D_4$ level of Tb^{3+} showed values of 4.3, 4.28, 4.28, 3.44, 1.42, and 1.01 ms when Eu^{3+} concentration increased to 0, 0.15, 0.3, 1.5, 8.5, and 14 mol%, respectively (see Table 1).
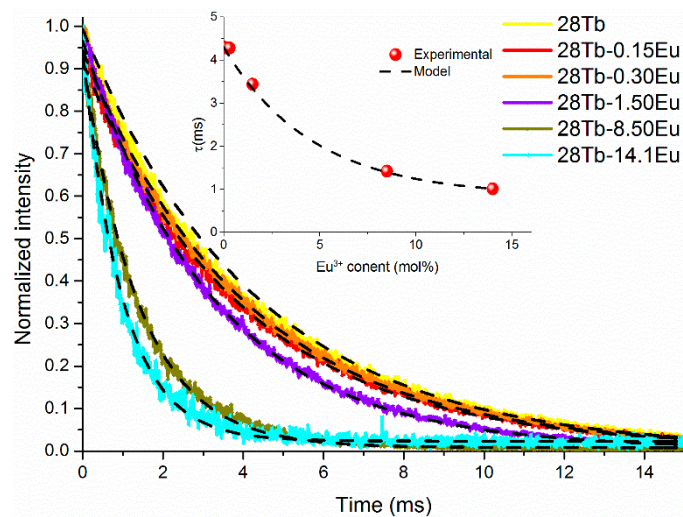
Figure 7. Experimental lifetime curves. The inset is a graph of experimental lifetime. Black lines represent the fitting model.

Figure 8 shows the experimental normalized emission spectra according to Equations (11) and 12. Additionally, adjustment of the experimental data was carried out using Equations (9) and (10), with B_{10} = 131.2/s. The model simultaneously adjusted the emission spectrum and lifetime curves. Luminescent efficiency can be defined by the ratio of population loss by emission and the population gain of the level:

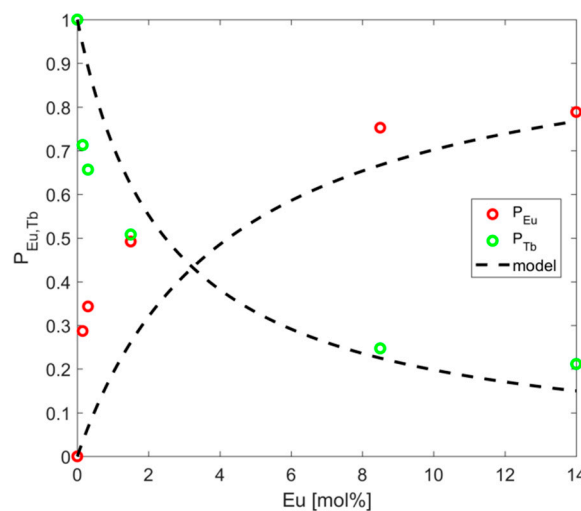$$\eta = \frac{A_{10}N_{Tb}^1}{A_{21}N_{Tb}^2} \tag{15}$$

Figure 8. Normalized emission spectrum related to the Eu^{3+} (red) and Tb^{3+} (green) ions. Black lines represent the fitting model.

Substituting Equations (4) and (5) we find:

$$\eta = \frac{A_{01}}{A_{01} + WN_{Eu}} \tag{16}$$

Energy transfer efficiency can be defined by the ratio of population loss by energy transfer and the population gain of the level:

$$ET = \frac{WN^1_{Tb}N^0_{Eu}}{A_{21}N^2_{Tb}} = \frac{WN_{Eu}}{A_{01} + WN_{Eu}} \tag{17}$$

Equations (16) and (17) fulfill the following relationship:

$$ET + \eta = 1 \tag{18}$$

Then, energy transfer can be rewritten as:

$$ET = 1 - \frac{\tau}{\tau_0} \tag{19}$$

where $\tau = (A_{01} + WN_{Eu})^{-1}$ is the lifetime, and $\tau_0 = (A_{01})^{-1}$ is the radiative lifetime. In this work, $\tau = \tau_{Tb-Eu}$ and $\tau_0 = \tau_{Tb}$ were the fluorescence lifetimes of the $^5D_4$ level of Tb^{3+} for Tb^{3+}-doped and Tb^{3+}/Eu^{3+}-codoped ceramic phosphor plates. The calculated ET efficiency increased from 5 to 76% when the Eu^{3+} concentration increased from 0.15 to 14 mol%. ET increased rapidly to 30% with the addition of 1.5 mol% of Eu^{3+}; after this concentration, no big changes were observed, and the ET was kept almost constant at 14 mol% of Eu^{3+}.

3.3. White Light Device Fabrication

Figure 9 shows multicolor light devices that were constructed using the Tb^{3+}/Eu^{3+}-codoped ceramic phosphor plate and the 380 nm UV LED chip.
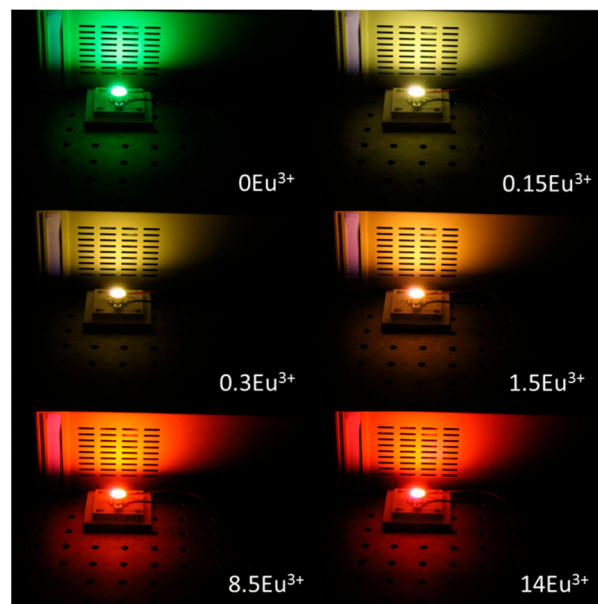

Figure 9. Luminescence photographs of fabricated devices under a 380 nm UV LED chip.

The electroluminescence of fabricated devices as a function of Eu^{3+} concentration with a bias current of 20 mA is shown in Figure 10. Representative samples with 0.15, 0.3, and 1.5 mol% of Eu^{3+} clearly showed 380 (UV LED), 544 (Tb^{3+}), 592 (Eu^{3+}), and 614 nm (Eu^{3+}) bands, where warm white was the feature color emissions of these devices. The maximum luminous efficacy was measured to be 13.08 lm/W for 28 mol% of Tb^{3+}, whereas a decrement from 9.22 to 6.04 lm/W was observed as the Eu^{3+} concentration increased (see Table 1). The low values of luminous efficacy were associated with the

opacity of the samples, the low efficiency of UV LED (InGaN), as well as the poor contribution of color from LED.
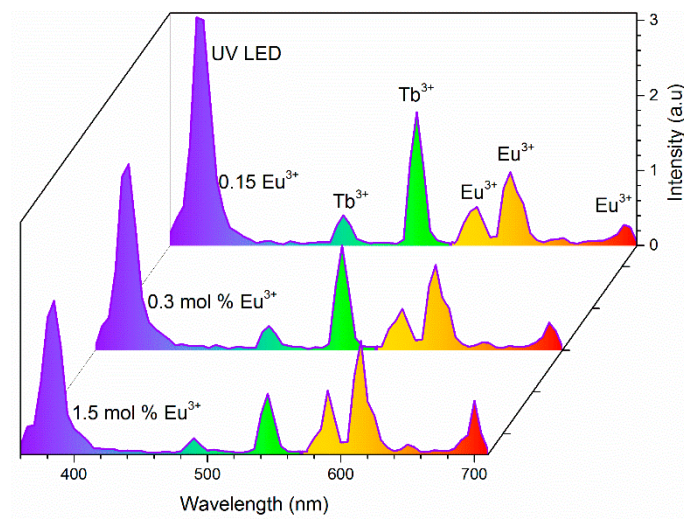

Figure 10. Electroluminescent spectra of LEDs fabricated using a 380 nm UV LED chip combined with Tb^{3+}-doped and Tb^{3+}/Eu^{3+}-codoped ceramic phosphor plates under a forward bias of 20 mA.

Figure 11 shows the color coordinates of the samples under study. The values were located on the edge of the chromaticity diagram, predominantly in yellow and red regions. The emitted color of the device changed from green to red through warm white by keeping the Tb^{3+} concentration and changing the Eu^{3+} content. The obtained results showed that the optical properties of LED were strongly influenced by Eu^{3+} content. Interestingly, by doping with only 0.15 mol% of Eu^{3+}, it was possible to modify both CRI and CCT. CRI showed an increase from 34 to 74.81, and CCT diminished from 5497 to 3658 K; these features were very adequate for indoor lighting. The samples with 0.3 and 1.5 mol% of Eu^{3+} gave the highest CRIs of approximately 82.5 and 82.6 with CCTs of 3136 and 2225 K, respectively. Although the luminous efficacy of the devices was low, we expected to further increase such values by introducing Tb^{3+} and Eu^{3+} in an adequate matrix or by codoping with Ce^{3+} to increase the absorption strength. The obtained results showed that by choosing properly the Eu^{3+} concentration, it was possible to produce comfortable white light devices for vivid applications in daily life.
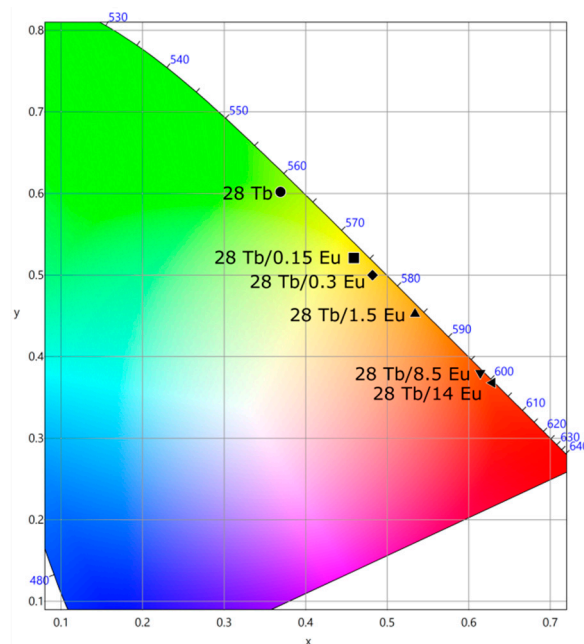
Figure 11. CIE diagram of chromaticity as function of Eu^{3+} content.

4. Conclusions

In summary, the fabrication of $LiYF_4$ ceramic phosphor plates doped with Tb^{3+}/Eu^{3+} ions is reported. The maximum excitation peak of a single Tb^{3+} was at 373 nm; however, this changed to 378 nm when $LiYF^4{:}10Tb^{3+}$ was codoped with Eu^{3+} ions. Based on the experimental results, it was concluded that intensity ratios between emission bands could be tuned by choosing properly the ion concentrations of both Tb^{3+} and Eu^{3+} ions. By placing the $LiYF_4{:}28Tb^{3+}/yEu^{3+}$ (mol%) ceramic phosphor plates on the top of 380 nm LED chip, green, warm, and red color emissions were obtained. It was found that warm white was achieved by adding only 0.15 mol% of Eu^{3+} without serious detriment to the luminous efficacy. However, when the concentration of Eu^{3+} increased to 0.3 mol% in $LiYF_4{:}28Tb^{3+}/yEu^{3+}$ (mol%), a CRI of 82.3 and a CCT of 3136 K were measured. With an increase in Eu^{3+} concentration, the yellow and red bands were improved, but the blue and green bands were reduced. Then, it was necessary to compromise CRI, CCT, and luminous efficacy to define the ion concentration. The obtained CRI was one of the highest reported in the literature for the Tb^{3+}/Eu^{3+} system, which, in combination with low CCT, made $LiYF_4$ ceramic phosphor plates a good candidate for solid-state lighting applications.

References

1. Fujita, S.; Yoshihara, S.; Sakamoto, A.; Yamamoto, S.; Tanabe, S. *YAG Glass-Ceramic Phosphor for White LED (I): Background and Development*; Ferguson, I.T., Carrano, J.C., Taguchi, T., Ashdown, I.E., Eds.; SPIE: San Diego, CA, USA, 2005; p. 594111.
2. Zhang, X.; Wang, J.; Huang, L.; Pan, F.; Chen, Y.; Lei, B.; Peng, M.; Wu, M. Tunable Luminescent Properties and Concentration-Dependent, Site-Preferable Distribution of Eu^{2+} Ions in Silicate Glass for White LEDs Applications. *ACS Appl. Mater. Interfaces* **2015**, *7*, 10044–10054. [CrossRef] [PubMed]

3. Fujita, S.; Sakamoto, A.; Tanabe, S. Luminescence Characteristics of YAG Glass–Ceramic Phosphor for White LED. *IEEE J. Sel. Top. Quantum Electron.* **2008**, *14*, 1387–1391. [CrossRef]

4. Lee, Y.K.; Lee, J.S.; Heo, J.; Im, W.B.; Chung, W.J. Phosphor in glasses with Pb-free silicate glass powders as robust color-converting materials for white LED applications. *Opt. Lett.* **2012**, *37*, 3276. [CrossRef] [PubMed]

5. Li, S.; Zhu, Q.; Wang, L.; Tang, D.; Cho, Y.; Liu, X.; Hirosaki, N.; Nishimura, T.; Sekiguchi, T.; Huang, Z.; et al. CaAlSiN$_3$:Eu^{2+} translucent ceramic: A promising robust and efficient red color converter for solid state laser displays and lighting. *J. Mater. Chem. C* **2016**, *4*, 8197–8205. [CrossRef]

6. Ji, E.-K.; Song, Y.-H.; Bak, S.H.; Jung, M.K.; Jeong, B.W.; Lee, D.B.; Yoon, D.-H. The design of a ceramic phosphor plate with functional materials for application in high power LEDs. *J. Mater. Chem. C* **2015**, *3*, 12390–12393. [CrossRef]

7. Ghoneim, N.A.; Halawa, M.M. Effect of boron oxide on the thermal conductivity of some sodium silicate glasses. *Thermochim. Acta* **1985**, *83*, 341–345. [CrossRef]

8. Hanna, B.; Bohn, R.G. Thermal Conductivity of Li$_2$O·Al$_2$O$_3$·nSiO$_2$ Glass—Ceramics between 5 and 100 K. *J. Am. Ceram. Soc.* **1991**, *74*, 3035–3038. [CrossRef]

9. Zhang, R.; Lin, H.; Yu, Y.; Chen, D.; Xu, J.; Wang, Y. A new-generation color converter for high-power white LED: Transparent Ce^{3+}:YAG phosphor-in-glass: Ce:YAG phosphor-in-glass for high-power white LED. *Laser Photonics Rev.* **2014**, *8*, 158–164. [CrossRef]

10. Yoo, H.; Kouhara, Y.; Yoon, H.C.; Park, S.J.; Oh, J.H.; Do, Y.R. Sn–P–F containing glass matrix for the fabrication of phosphor-in-glass for use in high power LEDs. *RSC Adv.* **2016**, *6*, 111640–111647. [CrossRef]

11. Kim, E.; Unithrattil, S.; Sohn, I.S.; Kim, S.J.; Chung, W.J.; Im, W.B. Facile one-step fabrication of 2-layered and 4-quadrant type phosphor-in-glass plates for white LEDs: An insight into angle dependent luminescence. *Opt. Mater. Express* **2016**, *6*, 804. [CrossRef]

12. Feldmann, C.; Jüstel, T.; Ronda, C.R.; Schmidt, P.J. Inorganic Luminescent Materials: 100 Years of Research and Application. *Adv. Funct. Mater.* **2003**, *13*, 511–516. [CrossRef]

13. Baur, F.; Glocker, F.; Jüstel, T. Photoluminescence and energy transfer rates and efficiencies in Eu^{3+} activated Tb$_2$Mo$_3$O$_{12}$. *J. Mater. Chem. C* **2015**, *3*, 2054–2064. [CrossRef]

14. Janulevicius, M.; Marmokas, P.; Misevicius, M.; Grigorjevaite, J.; Mikoliunaite, L.; Sakirzanovas, S.; Katelnikovas, A. Luminescence and luminescence quenching of highly efficient Y$_2$Mo$_4$O$_{15}$:Eu^{3+} phosphors and ceramics. *Sci. Rep.* **2016**, *6*, 26098. [CrossRef] [PubMed]

15. Zhu, C.; Chaussedent, S.; Liu, S.; Zhang, Y.; Monteil, A.; Gaumer, N.; Yue, Y. Composition dependence of luminescence of Eu^{3+} and Eu^{3+}/Tb^{3+} doped silicate glasses for LED applications. *J. Alloys Compd.* **2013**, *555*, 232–236. [CrossRef]

16. Zhu, C.; Wang, J.; Zhang, M.; Ren, X.; Shen, J.; Yue, Y. Eu-,Tb-, and Dy-Doped Oxyfluoride Silicate Glasses for LED Applications. *J. Am. Ceram. Soc.* **2014**, *97*, 854–861. [CrossRef]

17. Zhang, X.; Zhou, L.; Shi, J.; Gong, M. Luminescence and energy transfer of a color tunable phosphor Tb^{3+}, Eu^{3+} co-doped KCaY(PO$_4$)$_2$. *Mater. Lett.* **2014**, *137*, 32–35. [CrossRef]

18. Wang, B.; Ren, Q.; Hai, O.; Wu, X. Luminescence properties and energy transfer in Tb^{3+} and Eu^{3+} co-doped Ba$_2$P$_2$O$_7$ phosphors. *RSC Adv.* **2017**, *7*, 15222–15227. [CrossRef]

19. Xu, M.; Wang, L.; Jia, D.; Zhao, H. Tuning the Color Emission of Sr$_2$P$_2$O$_7$: Tb^{3+}, Eu^{3+} Phosphors Based on Energy Transfer. *J. Am. Ceram. Soc.* **2015**, *98*, 1536–1541. [CrossRef]

20. Jiang, T.; Yu, X.; Xu, X.; Yu, H.; Zhou, D.; Qiu, J. Realization of tunable emission via efficient Tb^{3+}–Eu^{3+} energy transfer in K$_3$Gd(PO$_4$)$_2$ for UV-excited white light-emitting-diodes. *Opt. Mater.* **2014**, *36*, 611–615. [CrossRef]

21. Zhang, X.; He, P.; Zhou, L.; Shi, J.; Gong, M. Energy transfer and luminescent properties of a green-to-red color tunable Tb^{3+}, Eu^{3+} co-doped K$_2$Y(WO$_4$)(PO$_4$) phosphor. *Mater. Res. Bull.* **2014**, *60*, 300–307. [CrossRef]

22. Xia, Y.; Huang, Y.; Long, Q.; Liao, S.; Gao, Y.; Liang, J.; Cai, J. Near-UV light excited Eu^{3+}, Tb^{3+}, Bi^{3+} co-doped LaPO$_4$ phosphors: Synthesis and enhancement of red emission for WLEDs. *Ceram. Int.* **2015**, *41*, 5525–5530. [CrossRef]

23. Zhang, B.; Zou, H.; Guan, H.; Dai, Y.; Song, Y.; Zhou, X.; Sheng, Y. Lu$_2$O$_2$S:Tb^{3+}, Eu^{3+} nanorods: Luminescence, energy transfer, and multicolour tuneable emission. *CrystEngComm* **2016**, *18*, 7620–7628. [CrossRef]

24. Huo, J.; Dong, L.; Lü, W.; Shao, B.; You, H. Novel tunable green-red-emitting oxynitride phosphors co-activated with Ce^{3+}, Tb^{3+}, and Eu^{3+}: Photoluminescence and energy transfer. *Phys. Chem. Chem. Phys.* **2017**, *19*, 17314–17323. [CrossRef] [PubMed]

25. Xia, Z.; Zhuang, J.; Liu, H.; Liao, L. Photoluminescence properties and energy transfer of Ba$_2$Lu(BO$_3$)$_2$Cl:Eu^{2+}/Eu^{3+}, Tb^{3+} phosphors. *J. Phys. Appl. Phys.* **2012**, *45*, 015302. [CrossRef]

26. Jiang, Y.; Xia, H.; Zhang, J.; Yang, S.; Jiang, H.; Chen, B. Growth and Optical Spectra of Tb^{3+}/Eu^{3+} Co-doped Cubic $NaYF_4$ Single Crystal for White Light Emitting Diode. *J. Mater. Sci. Technol.* **2015**, *31*, 1232–1236. [CrossRef]

27. Mahalingam, V.; Vetrone, F.; Naccache, R.; Speghini, A.; Capobianco, J.A. Colloidal Tm^{3+}/Yb^{3+}-Doped $LiYF_4$ Nanocrystals: Multiple Luminescence Spanning the UV to NIR Regions via Low-Energy Excitation. *Adv. Mater.* **2009**, *21*, 4025–4028. [CrossRef]

28. Kim, S.Y.; Won, Y.-H.; Jang, H.S. A Strategy to enhance Eu^{3+} emission from $LiYF_4$:Eu nanophosphors and green-to-orange multicolor tunable, transparent nanophosphor-polymer composites. *Sci. Rep.* **2015**, *5*, 7866. [CrossRef]

29. Szpikowska-Sroka, B.; Pawlik, N.; Goryczka, T.; Pisarski, W.A. Technological aspects for Tb^{3+}-doped luminescent sol-gel nanomaterials. *Ceram. Int.* **2015**, *41*, 11670–11679. [CrossRef]

30. Jiang, Y.; Xia, H.; Yang, S.; Zhang, J.; Jiang, D.; Wang, C.; Feng, Z.; Zhang, J.; Gu, X.; Zhang, J.; et al. Luminescence of Tb^{3+}/Eu^{3+} codoped $LiYF_4$ single crystals under UV excitation for white-light LEDs. *Chin. Opt. Lett.* **2015**, *13*, 071601. [CrossRef]

31. Zhang, S.; Li, Y.; Lv, Y.; Fan, L.; Hu, Y.; He, M. A full-color emitting phosphor $Ca_9Ce(PO_4)$ 7:Mn^{2+}, Tb^{3+}: Efficient energy transfer, stable thermal stability and high quantum efficiency. *Chem. Eng. J.* **2017**, *322*, 314–327. [CrossRef]

32. Ptacek, P.; Schäfer, H.; Kömpe, K.; Haase, M. Crystal Phase Control of Luminescing α-$NaGdF_4$:Eu^{3+} and β-$NaGdF_4$:Eu^{3+} Nanocrystals. *Adv. Funct. Mater.* **2007**, *17*, 3843–3848. [CrossRef]

33. Žukauskas, A.; Vaicekauskas, R.; Ivanauskas, F.; Vaitkevičius, H.; Shur, M.S. Spectral optimization of phosphor-conversion light-emitting diodes for ultimate color rendering. *Appl. Phys. Lett.* **2008**, *93*, 051115. [CrossRef]